Effect of MnO_2 Dopant on Properties of Na^+-β/β"-Al_2O_3 Solid Electrolyte Prepared by a Synthesizing-cum-sintering Process

Dae-Han LEE, Jin-Sik KIM, Young-Hyuk KIM, Sung-Ki LIM *

Department of Materials Chemistry and Engineering, Konkuk University, 120, Neungdong-ro, Gwangjin-gu, 143-701, Seoul, Republic of Korea

crossref http://dx.doi.org/10.5755/j02.ms.22612

Received 25January 2019; accepted 17 December 2019

In order to simplify the complexity of the conventional solid-state reaction process, Na^+-β/β″-Al_2O_3 as a fast Na^+-ionic conductive solid electrolyte was fabricated using a synthesizing-cum-sintering process combined with the double-zeta method, which is able to distribute a small amount of Li_2O more homogeneously in the Na_2O-Al_2O_3-Li_2O system. Additionally, in order to enhance the ionic conductivity, MnO_2 was used as a dopant to increase the Na^+-ion concentration on the conduction plane in the Na^+-β/β″-Al_2O_3 crystal structure. The relative sintered density increased with the synthesis temperature, ultimately reaching 99.7 % after synthesis at 1400 °C. The phase formation showed an overall β″-phase fraction over 90 %. The addition of MnO_2 had a positive effect on the phase formation, but a negative influence on the relative density resulting from the grain growth promotion effect. The highest ionic conductivity was observed at 1.74×10^{-1} S/cm (350 °C) for the sample sintered at 1600 °C with 0.5 wt.% MnO_2.

Keywords: Na^+-β/β"-Al_2O_3, solid electrolyte of NBBs, synthesizing-cum-sintering, duble-zeta process, MnO_2 dopant.

1. INTRODUCTION

As part of the drive towards reducing energy consumption, many studies have focused on the use of renewable energy, such as solar and wind sources. Due to the dependence of renewable energy on natural sources, energy storage methods that enable the efficient use of such energy sources, such as Na-beta batteries (NBBs), are particularly important. As the most widely-used solid electrolyte is based on Na^+-β/β″-Al_2O_3, this type of electrochemical device is often referred to as an NBBs. Due to their high round-trip efficiency, high energy density, and capability of providing energy for durations in the order of hours, NBBs technologies have been attracting increased attention for application to renewable energy storage [1 – 3]. Since the invention of NBBs in the late 1960s, Na^+-β/β″-Al_2O_3 has been the most common choice of a battery electrolyte, primarily due to its high ionic conductivity (typically 0.2 – 0.4 S/cm at 300 °C), excellent compatibility/chemical stability with the electrode materials, satisfactory mechanical strength, and low material cost [4].

Na^+-β/β″-Al_2O_3 exhibits excellent practical applicability because of its high ionic but low electronic conductivities. Na^+ ions act as charge carriers in Na^+-β/β″-Al_2O_3. There are two parent phases: β-Al_2O_3 has the theoretical formula $Na_2O{\cdot}11Al_2O_3$ or $NaAl_{11}O_{17}$, while that for β″-Al_2O_3 is either $Na_2O{\cdot}5Al_2O_3$ or $NaAl_5O_8$ [5 – 7]. According to the Na_2O-Al_2O_3 phase diagram proposed by Fally et al. [8], β + β"-Al_2O_3 phases coexist in that region corresponding to the formula $Na_2O{\cdot}nAl_2O_3$ ($5.33 \leq n \leq 8.5$). β"-Al_2O_3 has a rhombohedral structure with an R3m space group and lattice constants of a = 5.614 and c = 33.85 Å. In general, its a-axis is similar to that of β-Al_2O_3, while its c-axis is 1.5 times longer and the concentration of alkaline ions on its conduction plane is higher. Therefore, the β"-Al_2O_3 exhibits substantially higher ionic conductivity [5, 9]. Na^+-β″-Al_2O_3 is not stable and decomposes at temperatures above 1400 °C in the binary system Na_2O-Al_2O_3 [10], so cations whose ionic radii are less than 0.097 nm are usually doped to stabilize Na^+-β"-Al_2O_3, which has a conductivity five times higher than Na^+-β-Al_2O_3 [11]. Mg^{2+} and Li^+ ions such as a stabilizer for Na^+-β/β"-Al_2O_3 solid electrolyte have been the most widely used stabilizing cations. Li^+ ions are known to be more effective for Na^+-β″-Al_2O_3 formation than Mg^{2+} ions [12]. However, the behavior of the different stabilizing cations during phase formation have not yet been elucidated, so it is difficult to determine the precise effects that each stabilizer has on the phase formation and transformation.

The degree of homogeneity for small amounts of Li_2O and Na_2O is a significant factor affecting the rates of transformations and β"-Al_2O_3 formation. Homogeneous mixtures can be obtained through an atomic-scale reaction using wet chemical processes such as co-precipitation [13, 14] or the sol–gel method [15 – 19]. Nevertheless, these processes are not regarded as being useful due to certain drawbacks, namely, the difficulty of synthesizing and forming undesirable structures through these processes [13]. In a conventional solid-state reaction, the problem of achieving homogeneous and uniform mixing can be expected due to the inefficient mixing and dissimilarity of the particle sizes and shapes between the major and minor phases. In recent years, numerous studies have focused on understanding Na^+-β/β"-Al_2O_3/YSZ composite solid electrolyte via vapor-phase synthesis [20, 21] for NBBs.

* Corresponding author. Tel.: +82-2-450-3500; fax: +82-2-444-3490.
E-mail address: *sklim@konkuk.ac.kr* (S.K. Lim)

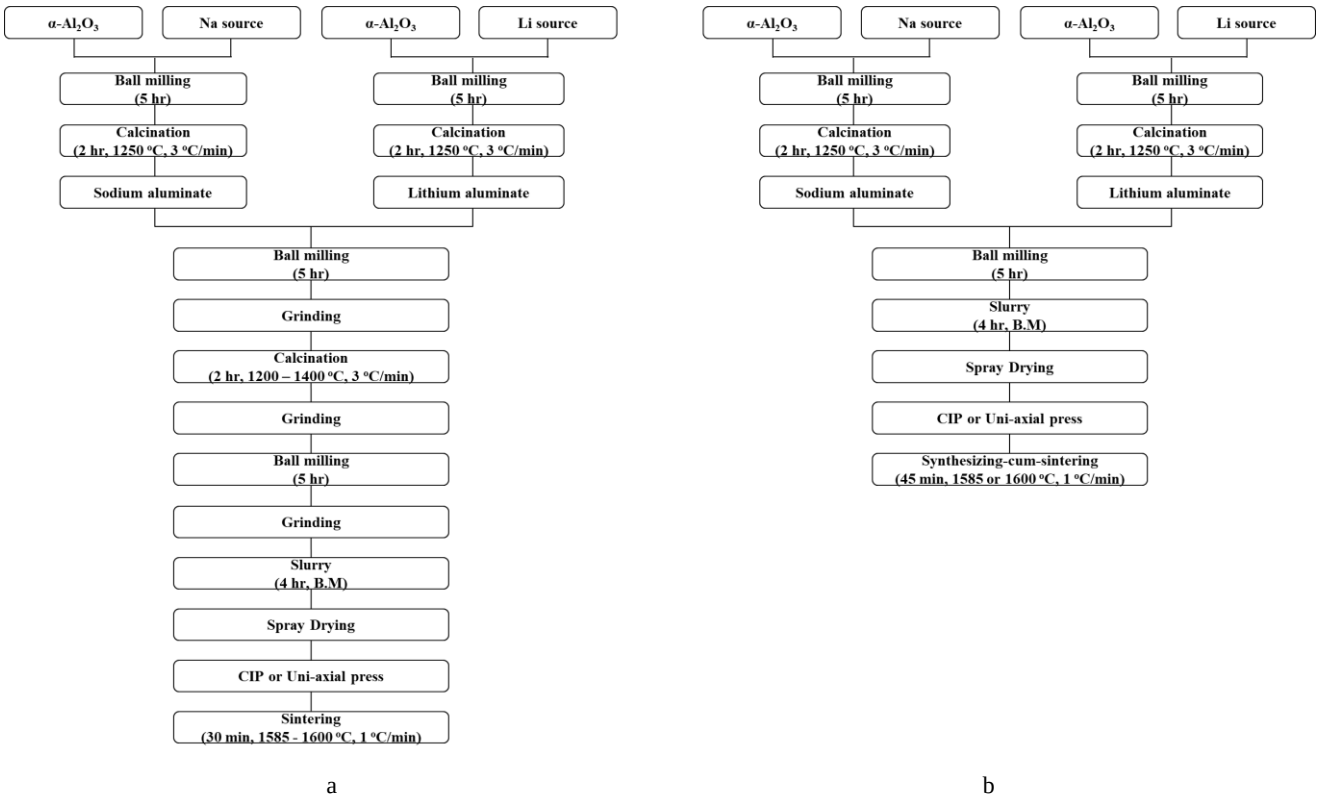

Fig. 1. Schematics of: a – double-zeta method; b – synthesizing-cum-sintering process combined with the double-zeta method

P. Parthasarathy et al [20] have reported that the mechanism of conversion involves a coupled transport of Na^+ ion through the Na^+-β″-Al_2O_3 and of O^{2-} ion through the YSZ. The kinetics of conversion has been investigated by measuring conversion thickness as a function of time [21]. Na^+-β″-Al_2O_3/YSZ composite samples prepared by vapor-phase synthesis have no liquid phase. These synthesized Na^+-β″-Al_2O_3/YSZ composites are also resistant to moisture-induced damage, unlike Na^+-β″-Al_2O_3 prepared by the conventional process. Sparks et al. [22] have studied dimensional geometrical changes and revealed the evolution of orientation degree of Na^+-β″-Al_2O_3 conduction plane. These Na^+-β″-Al_2O_3 phases have close-packed structures with three spinel blocks separated by 2-dimensional conduction planes containing Na^+ and O^{2-} ions. As a result, higher ionic conductivity is measured across sample thickness than that parallel to disc face. The ionic conductivity of Na^+-β″-Al_2O_3/YSZ composite via vapor-phase synthesis shows a close relationship with orientation degree of conduction plane such as [110] direction.

As mentioned above those problems of a conventional solid-state reaction can be improved by pre-diluting the minor constituents. In the so-called double-zeta process [23, 24], Li_2O is contained in the Li_2CO_3 in tiny quantities, but if it were in the form of $Li_2O{\cdot}5Al_2O_3$, the amount could be five times greater. The use of lithium aluminate as a stabilizer instead of Li_2CO_3 will result in a much better distribution of Li^+ in the mixture and also enhance the rate of conversion to the β"-Al_2O_3 phase. As a result of the reaction, sodium aluminate is also expected to disperse Na^+ ions uniformly in the mixture and lead to the thorough transformation of the β-phase to the β"-phase. Li_2CO_3, Na_2CO_3, and α-Al_2O_3 were used as raw materials for synthesizing zeta lithium aluminate and sodium aluminate. They were mixed to a molar ratio of 1:5 by ball milling and synthesized at 1250 °C.

In this study, in order to overcome the complexity of the conventional solid-state reaction, the double-zeta method was combined with the synthesizing-cum-sintering process, in which the synthesis and the sintering are performed in a single process.

The synthesizing-cum-sintering process is extremely advantageous in terms of cost in comparison to the conventional process. In the conventional process, the materials are calcined in advance to produce Na^+-β/β″-Al_2O_3. However, these steps are complex and very costly. The synthesizing-cum-sintering reduces the total number of production steps and produces a Na^+-β/β″-Al_2O_3 solid electrolyte more efficiently by combining the synthesizing and firing steps. Fig. 1. presents schematic illustrations of the conventional solid-state reaction process and the synthesizing-cum-sintering process combined with the double-zeta method for sintered Na^+-β/β″-Al_2O_3 specimens.

MnO_2 is known to greatly promote α-Al_2O_3 grain growth as well as the formation of spinel blocks [25 – 27]. MnO_2 has been reported as being present in the tetrahedral sites of β/β″-Al_2O_3 [28, 29]. In β″-Al_2O_3 stabilized by MnO_2, Mn^{2+} is substituted for Al^{3+} in the tetrahedral sites of the spinel blocks.

The resulting charge defects were compensated for by the additional Na^+ ions in the conduction planes, which resulted in a higher Na^+ concentration and β″-Al_2O_3 phase fraction [30]. However, there have been no studies to date addressing how MnO_2 affects the properties of sintered Na^+-β/β″-Al_2O_3 in the synthesizing-cum-sintering process when combined with the double-zeta method.

2. EXPERIMENTAL DETAILS

The starting chemicals were Na_2CO_3 (99.5 % High Purity Chemicals, Japan), Li_2CO_3 (99+% Sigma-Aldrich, USA), and α-Al_2O_3 (99.99 %, High Purity Chemicals, Japan). In order to prepare the precursors such as sodium aluminate and lithium aluminate, the starting materials were mixed by ball milling for 8 h using methanol as a liquid medium at a molar ratio of $[Na_2O]:[Al_2O_3] = 1:5$ and $[Li_2O]:[Al_2O_3] = 1:5$. Then, each mixture was calcined at 1250 °C for 2 h in MgO crucibles. To fabricate Na^+-β/β″-Al_2O_3, the two precursors were mixed and ball-milled for 5 h. The molar ratio of $[Na_2O]:[Al_2O_3]$ was 1:5, and the Li_2O (stabilizer) content was fixed to 0.55 wt.%, and any Al_2O_3 deficiency was compensated for by adding α-Al_2O_3. The slurries used in the granulation step contained 1.2 wt.% polyvinyl alcohol as a binder for the composite powder and 0.8 wt.% octyl alcohol as an anti-foaming agent in distilled water. The resulting slurry had a solid content of 50 wt.%. Granules were formed from the prepared slurry using a spray-drying technique under the conditions of an inlet temperature of 110 °C, an outlet temperature of 200 °C, and an atomizer spinning at 8000 rpm.

Specimens were prepared as disk-shaped pellets (diameter: 14 mm, thickness: 1.2 mm) using a uniaxial press to apply a pressure of 200 MPa. These specimens were then embedded in the Na^+-β″-Al_2O_3 powder in the crucible so as to prevent the loss of Na_2O in air. The firing schedule in the synthesizing-cum-sintering process consisted of two steps, namely, the synthesis of Na^+-β/β″-Al_2O_3 and sintering for the densification. The synthesis step was conducted for 2 h at 1200 – 1400 °C while the sintering step was conducted for 45 min at 1585 and 1600 °C.

Additionally, MnO_2 was added during the slurry manufacturing process, and the amount of MnO_2 added was varied from 0.3 to 1.0 wt.%. Specimens were fabricated and sintered through the application of the above process. In order to determine the effect of MnO_2, the synthesis temperature was fixed to 1400 °C and the sintering step was conducted at 1585 and 1600 °C, respectively. Table 1 lists the compositions and designations of the evaluated specimens.

The microstructure was determined using a scanning electron microscope (SEM; Model JSM-6380, JEOL, Japan), and the relative sintered density was calculated using the Archimedes method (ASTM 373-88). The phase compositions of the sintered specimens were measured using an X-ray diffractometer (D/max 2200, Rigaku, Japan). The XRD was operated at 40 kV and 30 mA using Cu Kα radiation. The relative phase composition was determined by calculating the line intensities of the well-separated peaks of each phase [31, 32].

$$\%\ \text{of}\ \alpha = f(\alpha)/\{f(\alpha)+f(\beta)+f(\beta'')\}\times 100 \quad (1)$$

$$\%\ \text{of}\ \beta = f(\beta)/\{f(\alpha)+f(\beta)+f(\beta'')\}\times 100 \quad (2)$$

$$\%\ \text{of}\ \beta'' = f(\beta'')/\{f(\alpha)+f(\beta)+f(\beta'')\}\times 100 \quad (3)$$

$$f(\alpha) = 1/2\{I_{\alpha(104)}\times 10/9 + I_{\alpha(113)}\} \quad (4)$$

$$f(\beta) = 1/3\{I_{\beta(102)}\times 10/3 + I_{\beta(206)}\times 10/3.5 + I_{\beta(107)}\times 10/5.5\} \quad (5)$$

$$f(\beta'') = 1/2\{I_{\beta(10\underline{11})}\times 10/4 + I_{\beta''(20\underline{10})}\times 10/8\} \quad (6)$$

where $I_{\alpha(104),\ \alpha(113)}$ = X-ray intensities of the (104), (113) planes of the α-Al_2O_3 phase, $I_{\beta(012),\ \beta(026),\ \beta(017)}$ = X-ray intensities of the (012), (026), (017) planes of the β-Al_2O_3 phase, and $I_{\beta''(01\underline{11}),\ \beta''(20\underline{10})}$ = X-ray intensities of the (01$\underline{11}$), (20$\underline{10}$) planes of the β"-Al_2O_3 phase.

Table 1. Denotations of sintered specimens

Denotation	Synthesis temperature, °C	Sintering temperature, °C	MnO_2 addition, wt.%
1200 – 1600	1200	1600	None
1250 – 1600	1250	1600	None
1300 – 1600	1300	1600	None
1350 – 1600	1350	1600	None
1400 – 1600	1400	1600	None
1200 – 1585	1200	1585	None
1250 – 1585	1250	1585	None
1300 – 1585	1300	1585	None
1350 – 1585	1350	1585	None
1400 – 1585	1400	1585	None
0.3 – 1600	1400	1600	0.3
0.5 – 1600	1400	1600	0.5
0.7 – 1600	1400	1600	0.7
1.0 – 1600	1400	1600	1.0
0.3 – 1585	1400	1585	0.3
0.5 – 1585	1400	1585	0.5
0.7-1585	1400	1585	0.7
1.0-1585	1400	1585	1.0

The ionic conductivities of the sintered specimens were measured using blocking silver electrodes with an electrochemical complex impedance analyzer (Zahner, IM6), over a frequency range of 0.1 Hz to 3 MHz and a temperature range of 25 to 350 °C. In general, the electronic conductivity of the Na^+-β/β"-Al_2O_3 is known to be ~10^{-9} S/cm, a negligible value. Therefore, the ionic conductivities were calculated using the following equation with the measured impedance value:

$$\sigma = L/(R_s \times A) \quad (7)$$

where σ, L, R_s and A denote the ionic conductivity, specimen thickness, impedance of the specimen, and electrode area, respectively

3. RESULTS AND DISCUSSION

Fig. 2 shows the XRD patterns of the synthesized sodium aluminate and lithium aluminate precursors. We can prove that the raw material was converted to aluminates by comparing the XRD patterns of the precursor with those of $NaAlO_2$ (JCPDS 33-1200), $NaAl_5O_8$ (JCPDS 31-1262, Na^+-β"-Al_2O_3), $NaAl_{11}O_{17}$ (JCPDS 31-1263, Na^+-β-Al_2O_3), and $LiAl_5O_8$ (JCPDS 87-1278). The XRD pattern of the sodium aluminate precursor shows that a phase transformation of α-Al_2O_3 to Na^+-β/β"-Al_2O_3 occurred without any α-Al_2O_3 remaining. The XRD patterns of the sintered specimens by a synthesizing-cum-sintering process exhibited growth of the (10$\underline{11}$) and (20$\underline{10}$) planes, which correspond to β"-Al_2O_3, respectively.

The effects of the synthesis and sintering temperatures on the phase formation and relative density are shown in Fig. 3 and Fig. 4, using XRD patterns and phase fraction analysis from the measured X-ray intensity data [31, 32]. Fig. 3 shows the XRD patterns according to various

synthesis temperatures and sintering temperatures at 1600 °C and 1585 °C, respectively. All of the XRD patterns appeared to be similar in shape, with the growth of the β"-Al_2O_3 peak such as the (10$\underline{11}$), (20$\underline{10}$) planes. These results show that the phase transformations of sodium aluminate and lithium aluminate precursors to Na^+-β/β"-Al_2O_3 occurred completely, and that the β"-Al_2O_3 peaks had higher intensities than the β-Al_2O_3 peaks. In addition, the significant secondary phases, such as sodium aluminate, were not observed in all specimens. The phase transformations of β-Al_2O_3 to β"-Al_2O_3 were slightly increased at higher synthesis temperatures. The stabilization of β"-Al_2O_3 basically involves the substitution of the Al^{3+} ions by the stabilizing cations, and the substation of the compensating Li^+ ions for the octahedral Al^{3+} ions in the spinel block [33 – 35]. Thus, it can be assumed that the β"-Al_2O_3 phase formation is mainly controlled by the diffusion of the stabilizing ions. In addition, higher synthesis temperatures increase the ionic diffusion, thereby enhancing the transformation of β-Al_2O_3 to β"-Al_2O_3, whereas the β″-Al_2O_3 phase fraction tends to decrease as the sintering temperature increases, because the volatilization of the Na_2O was augmented as the sintering temperature increased, resulting in Na_2O-loss and leading to the conversion of β″ to β to adjust the molar ratio in the Na^+-β/β″-Al_2O_3 structure (Fig. 4. and Table 2). In contrast, the relative density of the specimen was enhanced as the synthesis and sintering temperatures increased. In the conventional solid-state reaction process, it was confirmed that a high sintering temperature could enhance the relative density, but no effect was observed of the synthesis temperature on the relative density [36]. However, in this synthesizing-cum-sintering process, a high synthesis temperature led to an increase in the relative density. Therefore, SEM micrographs and the bulk density of the synthesized specimen prior to sintering were observed. Fig. 5 shows the microstructures of the specimens prior to sintering. The specimens synthesized at 1400 °C (Fig. 5 b) exhibited greater grain growth than those synthesized at 1200 °C (Fig. 5 a). Furthermore, their bulk densities were 17 % greater than the bulk densities of those synthesized at 1200 °C. This suggests that a pre-sintering effect occurred at a high synthesis temperature during the synthesizing-cum-sintering process.

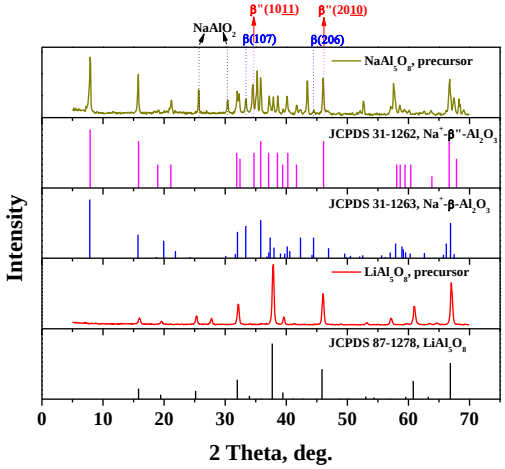

Fig. 2. X-ray diffraction patterns of calcined sodium and lithium aluminate precursors

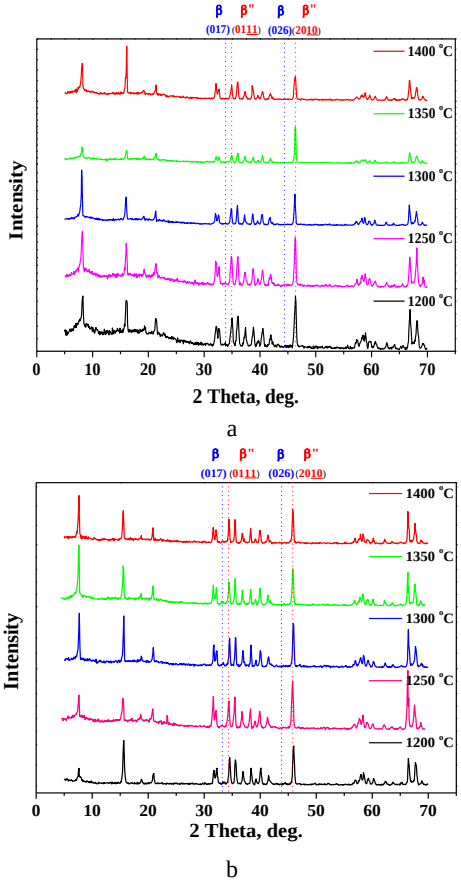

Fig. 3. X-ray diffraction patterns according to different synthesis and sintering temperatures. Sintered at: a – 1600 °C; b – 1585 °C

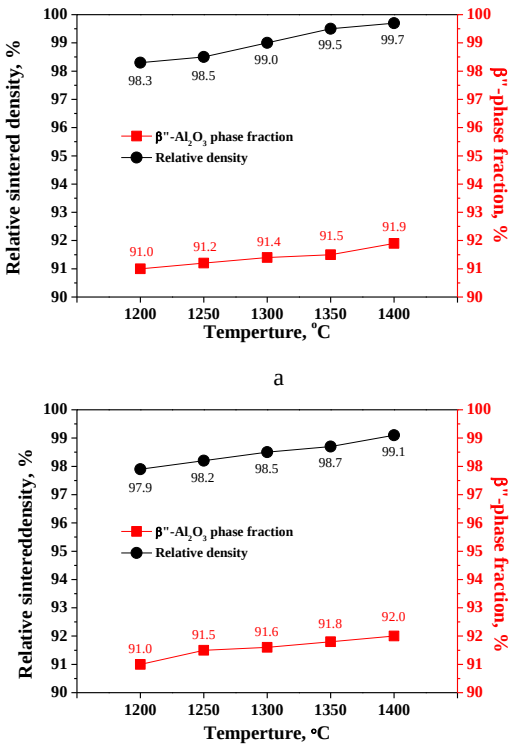

Fig. 4. The β″-Al_2O_3 phase fractions and relative density depending on synthesis temperatures. Sintered at: a – 1600 °C; b – 1585 °C

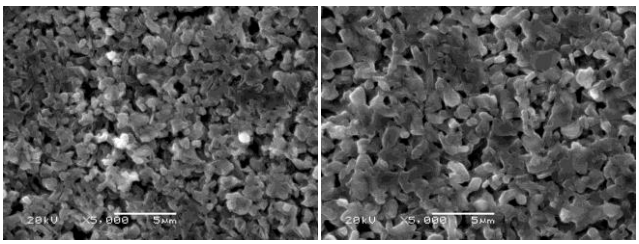

a b

Fig. 5. SEM images of specimens synthesized at: a – 1200 °C (bulk density: 1.99 g/cm^3); b – 1400 °C (bulk density: 2.33 g/cm^3)

The ionic conductivities of the specimens sintered at 1600 °C and 1585 °C after synthesis at several different temperatures were measured at 25 to 350 °C; these are shown in Fig. 6. The relationship conformed to Arrhenius equation of $\sigma T = Aexp(-E_a/kT)$, where A is the pre-exponential and k is the Boltzmann constant and T is the absolute temperature. As shown, the activation energy (slope of graph) declines when the temperature is above 250 °C. It means that the resistance of Na^+ ion conductivity can be improved as the temperature increasing [37]. Additionally, the specific resistance of each specimen at 350 °C is shown as a function of synthesis temperature in Fig. 7. The ionic conductivity was most affected by the β"-Al_2O_3 phase fraction and relative density. Among the samples, the maximum ionic conductivity measured for the 1400 – 1600 specimen was 1.25×10^{-1} S/cm at 350 °C, and the minimum ionic conductivity measured for the 1200 – 1585 specimen was 5.83×10^{-2} S/cm at 350 °C. This indicates that the synthesis and sintering temperatures in the synthesizing-cum-sintering process combined with the double-zeta method affected the ionic conductivity of Na^+-β/β″-Al_2O_3.

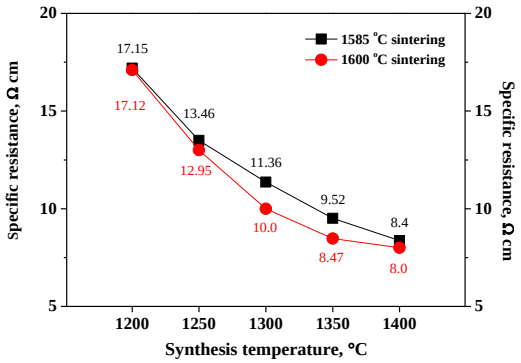

Fig. 7. Specific resistances of sintered specimens at 350 °C according to synthesis temperature

Specifically, a high synthesis temperature during the synthesizing-cum-sintering process positively influenced both the density and β″-Al_2O_3 phase. However, a high sintering temperature was effective for the densification while decreasing the β″-Al_2O_3 phase fraction, and consequently the ionic conductivity decreased. Table 2. summarizes the relative density, Na^+-β″-Al_2O_3 phase fraction, and ionic conductivity of each specimen.

Table 2. Relative density, β"-Al_2O_3 phase fraction, and ion conductivity according to synthesis and sintering temperature

Sintering temp., °C	Synthesis temp., °C	Relative density, %	β"-phase fraction, %	Ionic conductivity S/cm at 350 °C
1600	1200	98.3	91.0	5.84×10^{-2}
1600	1250	98.5	91.2	7.72×10^{-2}
1600	1300	99.0	91.4	1.00×10^{-1}
1600	1350	99.5	91.5	1.18×10^{-1}
1600	1400	99.7	91.9	1.25×10^{-1}
1585	1200	97.9	91.0	5.83×10^{-2}
1585	1250	98.2	91.5	7.43×10^{-2}
1585	1300	98.5	91.6	8.80×10^{-2}
1585	1350	98.7	91.8	1.05×10^{-1}
1585	1400	99.1	92.0	1.19×10^{-1}

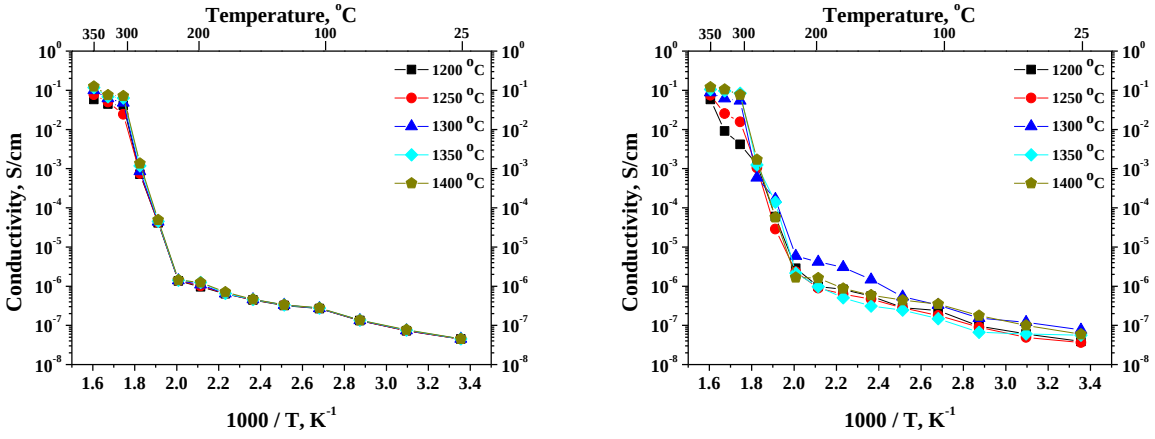

a b

Fig. 6. Ionic conductivity of specimens at 25 – 350 °C depending on synthesis temperature, sintered at: a – 1600 °C; b – 1585 °C

The XRD patterns corresponding to the addition of MnO_2 are shown in Fig. 8. The analysis was performed for the specimens sintered at 1600 °C and 1585 °C at a fixed synthesis temperature of 1400 °C, respectively. In addition, Fig. 9. shows the relative density and the β"-Al_2O_3 phase fraction, obtained through calculation from the measured X-ray intensity data.

In respect to the phase formation, the β"-Al_2O_3 phase fraction increased with the amount of MnO_2. The divalent cation Mn^{2+} in the MnO_2 strongly prefers a tetrahedral coordination environment in the β/β"-Al_2O_3 structure and accomplishes this by substituting Al^{3+} into Mn^{2+} in a tetrahedral site. The resulting charge defects lead to Al^{3+} ion vacancies, which favorably affects the formation of β"-Al_2O_3 phase due to the rapid diffusion of Na^+ and Al^{3+} ions [30, 36, 38]. In respect of the density, however, the addition of the MnO_2 formed an intergranular liquid phase which promoted grain growth. Consequently, rapid grain growth in the intergranular liquid phase led to pores between irregularly shaped grains [25, 26]. As a result, the addition of MnO_2 decreased the relative sintered density, as shown in Fig. 10. Fig. 10 a and c show SEM images of the specimens to which 0.3 % MnO_2 had been added at the sintering temperature of 1585 °C, while Fig. 10 b and d show the specimens to which 1.0 % MnO_2 had been added at 1600 °C. Comparing Fig. 10 a, c and Fig. 10 b, d to identify the effect of MnO_2, the addition of MnO_2 appears to cause grain growth with intergranular liquid phase.

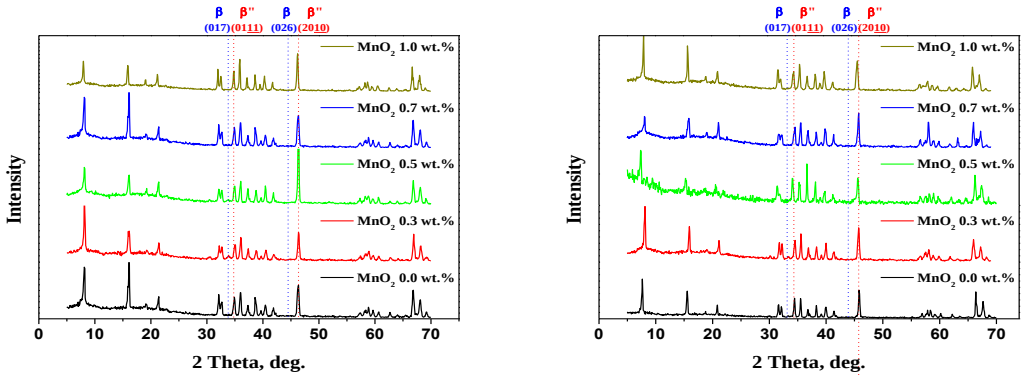

Fig. 8. X-ray diffraction patterns according to MnO_2 content. Synthesized at 1400 °C and sintered at: a – 1600 °C; b – 1585 °C

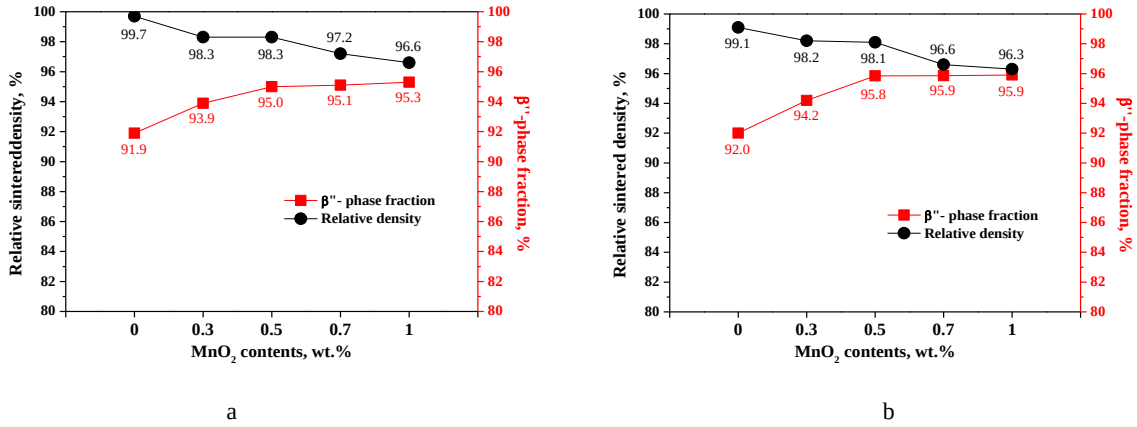

Fig. 9. β″-Al_2O_3 phase fractions and relative density according to MnO_2 content. Synthesized at 1400 °C and sintered at: a – 1600 °C; b – 1585 °C

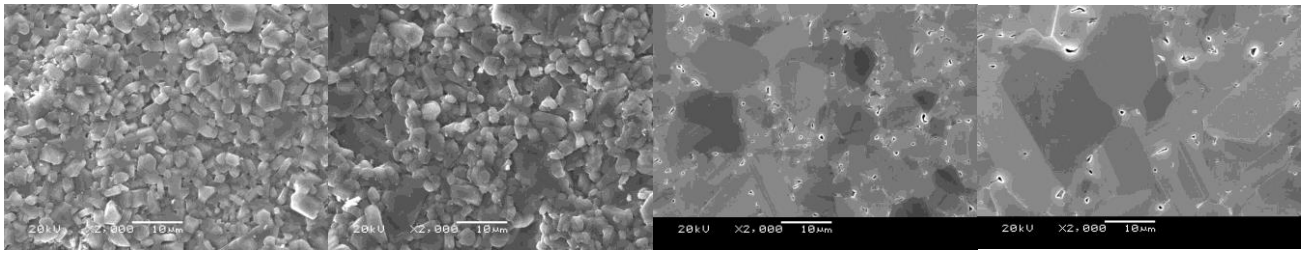

Fig. 10. SEM images of specimens: a – 0.3 – 1585 (R.D: 98.2 %); b – 1.0 – 1600 (R.D: 96.6 %); surface polished specimens: c – 0.3 – 1585; d – 1.0 – 1600 specimens

Fig. 11 shows the ionic conductivity of the MnO_2-doped Na^+-β/β"-Al_2O_3 specimens sintered at 1600 °C and 1585 °C, respectively, at 25 – 350 °C. Additionally, the specific resistance at 350 °C for each specimen is shown in Fig. 12 a. For example, Fig. 12 b shows the Nyquist plot of the 0.5 – 1600 and 1.0 – 1585 sintered specimens at 350 °C. The calculated specific resistance of the 1.0 – 1585 specimen appeared to be higher than that of the 0.5 – 1600 sintered specimen. In the case of Na^+-β/β"-Al_2O_3, the grain boundary contribution to the total resistance was negligible above 250 °C, and no semicircle corresponding to the grain boundary was observed at 350 °C. Table 3 conclusively summarizes the relative density, Na^+-β"-Al_2O_3 phase fraction, and ionic conductivity of each specimen. The ionic conductivity increased to a maximum of 1.74×10^{-1} S/cm until the MnO_2 concentration reached 0.5 wt.%. Thereafter, the ionic activity tended to decrease, because MnO_2 has an ambivalent effect on the ionic conductivity. The grain growth and high β"-Al_2O_3 phase fraction caused by the addition of MnO_2 improved the ionic conductivity, but due to the declining density, the ionic conductivities of the specimens with more than 0.5 wt.% MnO_2 decreased.

Table 3. Relative density, β"-Al_2O_3 phase fraction, and ion conductivity according to MnO_2 content and sintering temperature

Sintering temp., °C	MnO_2 contents, wt.%	Relative density, %	β"- phase fraction, %	Ionic conductivity S/cm at 350 °C
1600	0.0	99.7	91.9	1.25×10^{-2}
1600	0.3	98.3	93.9	1.31×10^{-1}
1600	0.5	98.3	95.0	1.74×10^{-1}
1600	0.7	97.2	95.1	1.34×10^{-1}
1600	1.0	96.6	95.3	9.37×10^{-2}
1585	0.0	99.1	92.0	1.19×10^{-1}
1585	0.3	98.2	94.2	1.23×10^{-1}
1585	0.5	98.1	95.8	1.56×10^{-1}
1585	0.7	96.6	95.9	1.02×10^{-1}
1585	1.0	96.3	95.9	7.99×10^{-2}

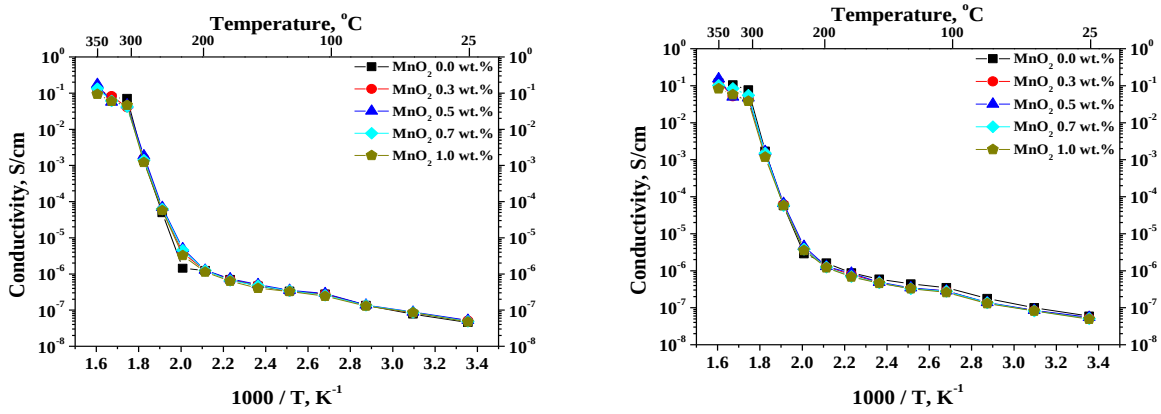

Fig. 11. Ionic conductivities of specimens sintered at: a – 1600 °C; b – 1585 °C as a function of the MnO_2 content at 25 – 350 °C

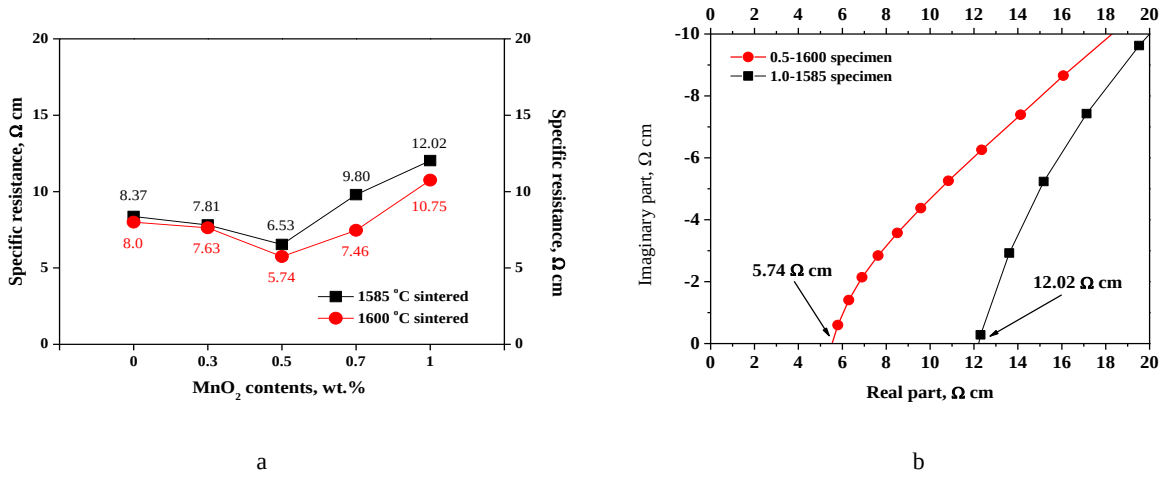

Fig. 12. Specific resistances of sintered specimens: a – as a function of MnO_2 content; b – Nyquist plot of 0.5 – 1600 and 1.0 – 1585 sintered specimen at 350 °C

4. CONCLUSIONS

In the present study, Na^+-β/β″-Al_2O_3 was successfully fabricated through a simplified synthesizing-cum-sintering process combined with the double-zeta method in order to reduce the sintering temperature to less than 1600 °C in a Na_2O-Al_2O_3-Li_2O system. The higher synthesis temperature of 1200 – 1400 °C resulted in the higher relative density of Na^+-β/β″-Al_2O_3 after sintering, which was caused by a pre-consolidation effect during the synthesis process at these temperatures, showing the bulk density at 1.99 – 2.33 g/cm^3. In addition, the β"-Al_2O_3 phase fraction increased slightly with the synthesis temperature, but this increase was not significant. The highest relative density of Na^+-β/β″-Al_2O_3 was 99.7 % for the sample synthesized at 1400 °C and sintered at 1600 °C, for which the ionic conductivity was 1.25×10^{-1} S/cm at 350 °C. The addition of MnO_2 as a dopant promoted the β"-Al_2O_3 phase formation, and the β"-Al_2O_3 phase fraction could be extended to 95.9 % with 1.0 wt.% MnO_2. However, the addition of an excessive amount of MnO_2 (more than 0.5 wt.%) led to a decrease in the ionic conductivity, owing to the formation of the secondary phase as well as a decrease in the relative density. Consequently, the highest ionic conductivity was 1.74×10^{-1} S/cm at 350 °C, which was attained after synthesis at 1400 °C and sintering at 1600 °C with 0.5 wt.% MnO_2.

Acknowledgments

This work was supported by the Korea Institute of Energy Technology Evaluation and Planning (KETEP) grant funded by the Korea government (No.20172420108430, Development of high-capacity technology of high-safety sodium-ferronickel chloride battery)

REFERENCES

1. **Barison, S., Fasolin, S., Mortalò, C., Boldrini, S., Fabrizio, M.** Effect of Precursors on β-Alumina Electrolyte Preparation *Journal of the European Ceramic Society* 35 (7) 2015: pp. 2099 – 2107. https://doi.org/10.1016/j.jeurceramsoc.2015.01.006
2. **Yang, L.P., Shan, S.J., Wei, X.L., Liu, X.M., Yang, H., Shen, X.D.** The Mechanical and Electrical Properties of ZrO_2–TiO_2–Na-β/β″-Alumina Composite Electrolyte Synthesized via a Citrate Sol–Gel Method *Ceramics International* 40 (7) 2014: pp. 9055 – 9060. https://doi.org/10.1016/j.ceramint.2014.01.118
3. **Oshima, T., Kajita, M., Okuno, A.** Development of Sodium-Sulfur Batteries *International Journal of Applied Ceramic Technology* 1 (3) 2004: pp. 269 – 276. https://doi.org/10.1111/j.1744-7402.2004.tb00179.x
4. **Lu, X., Xia, G., Lemmon, J.P., Yang, Z.** Advanced Materials for Sodium-Beta Alumina Batteries: Status, Challenges and Perspectives *Journal of Power Sources* 195 (9) 2010: pp. 2431 – 2442. https://doi.org/10.1016/j.jpowsour.2009.11.120
5. **Goro, Y., Kazutaka, S.** On the Structures of Alkali Polyaluminates *Bulletin of Chemical Society of Japan* 41 (1) 1968: pp. 93 – 99. https://doi.org/10.1246/bcsj.41.93
6. **Beevers, C.A., Ross, M.A.S.** The Crystal Structure of "Beta Alumina" $Na_2O{\cdot}11Al_2O_3$ *Zeitschrift für Kristallographie - Crystalline Materials* 97 (1 – 6) 1937: pp. 59 – 66. https://doi.org/10.1524/zkri.1937.97.1.59
7. **Yao, Y.Y., Kummer, J.T.** Ion Exchange Properties of and Rates of Ionic Diffusion in Beta-Alumina *Journal of Inorganic and Nuclear Chemistry* 29 (9) 1967: pp. 2453 – 2466. https://doi.org/10.1016/0022-1902(67)80301-4
8. **Fally, J., Lasne, C., Lazennec, Y., Margotin, P.** Some Aspects of Sodium-Sulfur Cell Operation *Journal of the Electrochemical Society* 120 (10) 1973: pp. 1292 – 1295. https://doi.org/10.1149/1.2403249
9. **Kroon, A.P., Schaefer, G.W., Aldinger, F.** Direct Synthesis of Binary K-β- and K-β"-Alumina. 1. Phase Relations and Influence of Precursor Chemistry *Chemistry of Materials* 7 (5) 1995: pp. 878 – 887. https://doi.org/10.1021/cm00053a011
10. **Hodge, J.D.** Phase Relations in the System Na_2O-Li_2O-Al_2O_3 *Journal of American Ceramic Society* 67 1984: pp. 183 – 185. https://doi.org/10.1111/j.1151-2916.1984.tb19738.x|
11. **Imai, A., Harata, M.** Ionic Conduction of Impurity-Doped β-Alumina Ceramics *Japanese Journal of Applied Physics* 11 1972: pp. 180 – 185. https://doi.org/10.1143/JJAP.11.180
12. **Bera, J.** On the Transformation Kinetics of β – *to* β"-Alumina in the System Al_2O_3-Na_2O-Li_2O *Journal of Materials Science Letters* 12 1993: pp. 27 – 29.
13. **Hodge, J.D.** Kinetics of the β″-to-β Transformation in the System Na_2O-$A1_2O_3$ *Journal of American Ceramic Society* 66 (3) 1983: pp. 166 – 169. https://doi.org/10.1111/j.1151-2916.1983.tb10009.x
14. **Takahashi, T., Kuwabara, K.** β-Al_2O_3 Synthesis from m-Al_2O_3 *Journal of Applied Electrochemistry* 10 (3) 1980: pp. 291 – 297. https://doi.org/10.1007/BF00617203
15. **Morgan, P.E.D.** Low Temperature Synthetic Studies of Beta-Aluminas *Materials Research Bulletin* 11 (2) 1976: pp. 233 – 241. https://doi.org/10.1016/0025-5408(76)90080-5
16. **Yoldas, B.E., Partlow, D.P.** Formation of Continuous Beta Alumina Films and Coatings at Low Temperatures *American Ceramic Society Bulletin* 59 (6) 1980: pp. 640 – 642.
17. **Zaharescu, M., Parlog, C., Stancovschi, V., Crisan, D., Braileanu, A.** The Influence of the Powders Synthesis Method on the Microstructure of Lanthanum-Stabilized β-Alumina Ceramics *Solid State Ionics* 15 1985: pp. 55 – 60. https://doi.org/10.1016/0167-2738(85)90107-9
18. **Yamaguchi, S., Terabe, K., Iguchi, Y., Imai, A.** Formation and Crystallization of Beta-Alumina from Precursor Prepared by Sol-Gel Method Using Metal Alkoxides *Solid State Ionics* 24 (2 – 3) 1987: pp. 171 – 176. https://doi.org/10.1016/0167-2738(87)90117-2
19. **Jayaraman, V., Gnanasekaran, T., Periaswami, G.** Low-Temperature Synthesis of β-Aluminas by a Sol-Gel Technique *Materials Letters* 30 (2 – 3) 1997: pp. 157 – 162. https://doi.org/10.1016/S0167-577X(96)00193-0
20. **Parthasarathy, P., Virkar, A.V.** Vapor Phase Conversion of α-Alumina + Zirconia Composites into Sodium Ion Conducting Na-β″-Alumina + Zirconia Solid Electrolytes *Journal of Electrochemistry Society* 160 (11) 2013: pp. A2268 – A2280. http://dx.doi.org/10.1149/2.095311jes

21. **Ghadbeigi, L., Szendrei, A., Moreno, P., Sparks, T.D., Virkar, A.V.** Synthesis of Iron-Doped Na-β"-alumina + Yttria-Stabilized Zirconia Composite Electrolytes by a Vapor Phase Process *Solid State Ionics* 290 2016: pp. 77 – 82. http://dx.doi.org/10.1016/j. ssi.2016.04.006.
22. **Sparks, T.D., Ghadbeigi, L.** Anisotropic Properties of Na-β″-Alumina + YSZ Composite Synthesized by Vapor Phase Method *Journal of Materials Research* 33 (1) 2018: pp. 81 – 89. http://dx. doi.org/10.1557/jmr.2017.436.
23. **Youngblood, G.E., Virkar, A.V., Cannon, W.R., Gordon, R.S.** Sintering Process and Heat Treatment Schedules for Conductive, Lithia-Stabilized Beta Double Prime-Al_2O_3 *American Ceramic Society Bulletin* 56 (2) 1977: pp. 206 – 210.
24. **Wen, Z., Cao, J., Gu, Z., Xu, X., Zhang, F., Lin, Z.** Research on Sodium Sulfur Battery for Energy Storage *Solid State Ionics* 179 (27 – 32) 2008: pp. 1697 – 1701. https://doi.org/10.1016/j.ssi.2008.01.070
25. **Erkalfa, H., Misirli, Z., Demirci, M., Toy, C., Baykara, T.** The Densification and Microstructural Development of Al_2O_3 with Manganese Oxide Addition *Journal of European Ceramic Society* 15 (2) 1995: pp. 165 – 171. https://doi.org/10.1016/0955-2219(95)93062-8
26. **Erkalfa, H., Misirli, Z., Baykara, T.** The Effect of TiO_2 and MnO_2 on Densification and Microstructural Development of Alumina *Ceramics International* 24 (2) 1998: pp. 81 – 90. https://doi.org/10.1016/S0272-8842(97)00082-5
27. **German, R.M.** Liquid Phase Sintering, 1st ed., Springer US. New York, 1985: pp. 127 – 155. https://doi.org/10.1007/978-1-4899-3599-1
28. **Boilot, J.P., Kahn, A., Thery, J., Collongues, R., Antoine, J., Vivien, D., Chevrette, C., Gourier, D.** Influence of Foreign Ions Addition on Relative Stability and Electrical Conductivity of β and β" Alumina Type Phases Localization of Impurities *International Symposium on Solid Ionic and Ionic-Electronic Conductors* 1977: pp. 741 – 745. https://doi.org/10.1016/0013-4686(77)80029-7
29. **Geller, S.** Solid Electrolytes, 1st ed. Springer-Verlag Berlin Heidelberg Berlin, 1977: pp. 105 – 141. https://doi.org/10.1007/3-540-08338-3
30. **Wasiucionek, M., Garbarczyk, J., Jakubowski, W.** Electrical Properties of CoO, NiO, CuO and ZnO Doped Beta″-Alumina *Solid State Ionics* 7 (4) 1982: pp. 283 – 286. https://doi.org/10.1016/0167-2738(82)90024-8
31. **Li, J., Ye, Y.** Densification and Grain Growth of Al_2O_3 Nanoceramics during Pressureless Sintering *Journal of American Ceramic Society* 89 (1) 2006: pp. 139 – 143. https://doi.org/10.1111/j.1551-2916.2005.00654.x
32. **Xie, L., Cormack, A.N.** Cation Distribution in Magnetoplumbite and β″-Alumina Structures *Materials Letters* 9 (11) 1990: pp. 474 – 479. https://doi.org/10.1016/0167-577X(90)90121-2
33. **Collin, G., Boilot, J.P., Colomban, P., Comes, R.** Host Lattices and Superionic Properties in *β*- and β"-Alumina. I. Structures and Local Correlations *Physical Review B* 34 (8) 1986: pp. 5838 – 5849. https://doi.org/10.1103/PhysRevB.34.5838
34. **Bera, J.** Structure Analysis of β″-Alumina in Syntaxy with β-Alumina by Two-Stage X-Ray Powder Diffractometry *Solid State Communications* 82 (3) 1992: pp. 205 – 210. https://doi.org/10.1016/0038-1098(92)90265-B
35. **Reser, M.K.** Phase Diagrams for Ceramics, 2nd ed., The American Ceramic Society Inc. 1979: pp. 114(4th printing).
36. **Mak, T.C.W., Zou, G.D.** Crystallography in Modern Chemistry 1st ed. Wiley-Interscience, New York, 1992.
37. **Xu, D., Jiang, H., Li, M., Hai, O., Zhang, Y.** Synthesis and Characterization of Y_2O_3 Doped Na–β″-Al_2O_3 Solid Electrolyte by Double Zeta Process *Ceramics International* 41 2015: pp. 5355 – 5361. https://doi.org/10.1016/j.ceramint.2014.12.094
38. **Akridge, J.R., Kennedy, J.H.** Absorption and Emission Spectroscopy and Magnetic Susceptibility of Sodium β-Alumina Doped with Mn, Co, and Ni *Journal of Solid State Chemistry* 29 (1) 1979: pp. 63 – 72. https://doi.org/10.1016/0022-4596(79)90209-3